RESEARCH

Bacteriophage as a potential therapy to control antibiotic-resistant *Pseudomonas aeruginosa* infection through topical application onto a full-thickness wound in a rat model

Nouran Rezk[1], Abdallah S. Abdelsattar[1,2], Doaa Elzoghby[1], Mona M. Agwa[3], Mohamed Abdelmoteleb[4], Rania G. Aly[5], Mohamed S. Fayez[1], Kareem Essam[1], Bishoy M. Zaki[6] and Ayman El-Shibiny[1,7*]

Abstract

Background: Antibiotic-resistant *Pseudomonas aeruginosa* (*P. aeruginosa*) is one of the most critical pathogens in wound infections, causing high mortality and morbidity in severe cases. However, bacteriophage therapy is a potential alternative to antibiotics against *P. aeruginosa*. Therefore, this study aimed to isolate a novel phage targeting *P. aeruginosa* and examine its efficacy in vitro and in vivo.

Results: The morphometric and genomic analyses revealed that ZCPA1 belongs to the *Siphoviridae* family and could infect 58% of the tested antibiotic-resistant *P. aeruginosa* clinical isolates. The phage ZCPA1 exhibited thermal stability at 37 °C, and then, it decreased gradually at 50 °C and 60 °C. At the same time, it dropped significantly at 70 °C, and the phage was undetectable at 80 °C. Moreover, the phage ZCPA1 exhibited no significant titer reduction at a wide range of pH values (4–10) with maximum activity at pH 7. In addition, it was stable for 45 min under UV light with one log reduction after 1 h. Also, it displayed significant lytic activity and biofilm elimination against *P. aeruginosa* by inhibiting bacterial growth in vitro in a dose-dependent pattern with a complete reduction of the bacterial growth at a multiplicity of infection (MOI) of 100. In addition, *P. aeruginosa*-infected wounds treated with phages displayed 100% wound closure with a high quality of regenerated skin compared to the untreated and gentamicin-treated groups due to the complete elimination of bacterial infection.

Conclusion: The phage ZCPA1 exhibited high lytic activity against MDR *P. aeruginosa* planktonic and biofilms. In addition, phage ZCPA1 showed complete wound healing in the rat model. Hence, this research demonstrates the potential of phage therapy as a promising alternative in treating MDR *P. aeruginosa*.

Keywords: *Pseudomonas aeruginosa*, Multi-drug resistant (MDR), Wound infection, In vivo, Bacteriophage, Biofilm, Phage characterization, Phage isolation, Immunohistochemical (IHC)

Background

Pseudomonas aeruginosa (*P. aeruginosa*) is a Gram-negative, rod-shaped, aerobic, opportunistic pathogen responsible for 10% of hospital-acquired infections worldwide [1]. *P. aeruginosa* is a primary cause of pneumonia, wound infections, urinary tract infections, and bacteremia [2]. Antibiotics used to treat *P. aeruginosa* infections became ineffective due to worldwide

*Correspondence: aelshibiny@zewailcity.edu.eg

[7] Faculty of Environmental Agricultural Sciences, Arish University, Arish 45511, Egypt
Full list of author information is available at the end of the article

Rezk *et al. Journal of Genetic Engineering and Biotechnology*   (2022) 20:133

Page 2 of 16

antimicrobial resistance. It was estimated in 2019 that about 5 million deaths were because of antibiotic-resistant bacterial infections [3]. Moreover, the World Health Organization (WHO) indicated that antimicrobial-resistant bacterial infections could kill approximately 10 million people per year by 2050 [4]. In addition, WHO has classified it as a critical pathogen that requires immediate attention to develop new antibiotics [1].

P. aeruginosa has a high ability to develop resistance against a wide range of antibiotics, including fluoroquinolones, aminoglycosides, β-lactams, and different disinfectants. This is because it contains intrinsic and acquired mechanisms. The intrinsic resistance of *P. aeruginosa* includes reduction of membrane permeability, overexpression of efflux pumps that pump antibiotics out of the cell, and the production of antibiotic-degrading enzymes, including AmpC β-lactamases and aminoglycoside-modifying enzymes [5, 6]. Moreover, biofilm development is considered one of the primary resistance mechanisms in *P. aeruginosa*. *P. aeruginosa* biofilms are critical in protecting bacteria from host immune responses and are up to 1000 times more resistant to antibiotics than planktonic cells [7, 8]. Multidrug-resistant (MDR) *P. aeruginosa* has been linked to nosocomial infections and outbreaks in burn and intensive care units [9–11] and is a growing cause of hospital-acquired infections [12]. *P. aeruginosa* is also considered a severe threat by the Centers for Disease Control and Prevention (CDC) because of its high mortality rate [13]. Moreover, Egypt has the highest MDR *P. aeruginosa* prevalence (75.6%) in the Middle East (MENA) region [14].

Skin is the first defense barrier against bacterial infections, and any damage to the skin allows pathogens to enter the body, resulting in sepsis and death [15]. Wounds and skin damage can be induced by chemical and physical agents and diseases like diabetes [16]. Wound infection is one of the most common nosocomial infections with a high mortality rate [17]. *P. aeruginosa* is the most frequent driver of wound infections, which colonizes the wound site followed by expansion into internal organs through the bloodstream that ends with skin necrosis and serious complications and, in severe cases, can be life-threatening [16, 18, 19]. Moreover, *P. aeruginosa* is a significant cause of delayed wound healing. A meta-analysis study showed that 78.2% of biofilms in chronic non-healing wounds were associated with poor wound healing [20, 21]. According to Ijaz et al., MDR *P. aeruginosa* was found in 58.6% of clinical samples from wounded patients [22]. Therefore, better therapeutic and prophylactic treatments for combating MDR *P. aeruginosa* wound infections are required.

Phage therapy is one of the promising alternatives to antibiotics, which utilizes naturally occurring phages that are considered part of the human microbiome [23, 24] and have high specificity towards their bacterial hosts, including biofilm-forming and antibiotic-resistant bacteria [25–27]. Many research studies have highlighted the use of phages to control biofilm-forming bacteria, including *P. aeruginosa* and demonstrated the ability of phages to eradicate the *P. aeruginosa* infections [28, 29] and biofilm-forming bacterial cells [16, 30–33]. However, previous studies have focused mainly on the treatment of cystic fibrosis caused by *P. aeruginosa* by phages in vivo [29, 34–36]. Moreover, using phage therapy against MDR *P. aeruginosa* in wound infection shows high efficacy and safety through topical and oral administrations [29, 37–39]. Hence, this study aimed to isolate and characterize a novel phage against MDR *P. aeruginosa* from Egyptian clinical isolates and study its efficacy in vitro and on infected wounds using a rat model through single and multiple doses.

Methods
Bacterial characterization
Bacterial growth conditions

Fifty clinical wound swabs were collected from patients in Egyptian hospitals infected with P. aeruginosa and given as a gift to the Center for Microbiology and Phage therapy at Zewail City for Science and Technology. First, the clinical isolates were streaked on Cetrimide agar (Oxoid, England), and P. aeruginosa was identified according to the standard morphology on cetrimide agar that appears fluorescent green. Then, five colonies were picked for purification and stored in Tryptic Soy Broth (TSB; Oxoid, England) containing 20% (v/v) glycerol for storage at −80 °C. Before each experiment, fresh bacterial cultures were prepared by inoculating a single colony from Cetrimide agar into 1 mL of TSB in 1.5-mL Eppendorf and incubating for 16 h at 37 °C with shaking at 200 rpm. All methods were performed following the relevant guidelines and regulations.

Detection of P. aeruginosa and virulence genes using polymerase chain reaction (PCR)

According to the manufacturer's instructions, the bacterial DNA was extracted by QIAamp DNA Mini Kit (Qiagen, Germany). Seven virulence genes were used to confirm the pathogenicity and antibiotic resistance of the bacterial strains. Briefly, the total volume of each reaction was 25 μL containing 12.5 μL of 2x master mix (Thermo Scientific), 1 μL from each stock primer, 2 μL of bacterial DNA, 0.5 μL of 50 mM $MgCl_2$, and 8 μL of distilled water. Afterwards, the products were run through 1% (w/v) agarose gel (Sigma-Aldrich, USA) to determine the size of the PCR product. All the primer sequences, the predicted sizes, and annealing temperatures are shown in Table 1.

Rezk *et al. Journal of Genetic Engineering and Biotechnology*   (2022) 20:133

Page 3 of 16

Table 1 Primer set sequences for the seven virulence and resistance genes

Primer	Sequence	Product size (bp)	Annealing temperature (°C)	References
ETA	F: GACAACGCCCTCAGCATCACCAGC	396	60	[40]
	R: CGCTGGCCCATTCGCTCCAGCGCT			
PhzI	F: CATCAGCTTAGCAATCCC	392	50	[41]
	R: CGGAGAAACTTTTCCCTC			
PhzII	F: GCCAAGGTTTGTTGTCGG	1,036	51	[41]
	R: CGCATTGACGATATGGAAC			
bla-TEM	F: ATGAGTATTCAACATTTCCG	867	50	[42]
	R: CTGACAGTTACCAATGCTTA			
OprL	F: CGTGCGATCACCACCTTCTA	171	52.5	Designed for this study
	R: CTCGCCCAGAGCCATATTGT			
ExoS	F: GCCTTGTCGAGTCCCTTCAA	345	53.5	Designed for this study
	R: GCTTCAGCAGAGTCCGTCTT			
PlcH	F: CCTGACTTCGCTGTTCGACT	680	53.5	Designed for this study
	R: CCTGGTTCGGTTCGAGTTCA			

Antimicrobial susceptibility testing

The antibiotic profile of fifty *P. aeruginosa* isolates was investigated using the disc diffusion method [35]. The tested antibiotics were ciprofloxacin (CIP; 5 μg), gentamicin (CN; 10 μg), imipenem (IPM; 10 μg), cefepime (Feb; 30 μg), levofloxacin (LEV; 5 μg), amikacin (AK;30 μg), piperacillin (PRL; 10 μg), and meropenem (MEL; 5 μg) (Oxoid, UK). The diameter of the clear zone was measured, and the results were interpreted based on the Clinical and Laboratory Standards Institute (CLSI) [43].

16S rRNA gene sequencing

A second PCR reaction was performed to identify the bacterial strain *P. aeruginosa* (*P.s* 12), the primary host for further phage isolation and other studies using 16S rRNA gene sequencing. The PCR reaction volume was 50 μL, including 25 μL of 1x Master Mix (Thermo Scientific, USA), 5 μL of DNA sample was extracted by QIAamp DNA 93 Mini Kit (Qiagen, Germany), and 18 μL of nuclease-free water, and 1 μL of the forward primer (5′-AGAGTTTGATCCTGGCTCAG-3′), 1 μL of the reverse primer (5′-TACGGYTACCTTGTTACGACTT-3′). PCR program was 94 °C for 3 min, 30 cycles at 94 °C for 30 s, 55 °C for 30 s, 72 °C for 1 min, and 72 °C for 10 min. In addition, 1.5 % (v/w) of the agarose gel was used in gel electrophoresis for the separation of the PCR product, and gel purification was performed of 16s rRNA gene using QIAEX II Gel Extraction Kit (QIAGEN, Germany) as described in the manufacturer's protocol [41].

The 16S rRNA sequence was determined with a model 373A automated fluorescent-DNA sequencer (Applied Biosystem, USA). The nucleotide sequence of the 16s rRNA gene that was obtained was processed through Finch TV software (https://digitalworldbiology.com/FinchTV). BLASTN (Basic Local Alignment Search Tool, (http://www.ncbi.nlm.nih.gov/BLAST/Blast.cgi) against the 16S ribosomal RNA database was performed to identify the isolated strain [44]. The 16S rRNA sequence was deposited in the NCBI GenBank under accession number OL375153.

Phage isolation, purification, and propagation

More than ten sewage samples were taken from raw sewage, primary and secondary treatment stages from two different sewage treatment stations in Giza, Egypt. The samples were used for phage isolation using enrichment techniques [45, 46]. Briefly, 1mL of overnight culture from *P.s* 12 was added to 9 mL of sewage samples and incubated at 37 °C for 4h, 1% of chloroform was added to the mixture and centrifuged at 5000 rpm for 20 min, and the supernatant was retained. Afterwards, a spot assay was used by mixing 100 μl of exponential-phase bacterial host culture with 4 mL of soft agar (0.3% w/v agar), which was held at 55 °C, used at a suitable temperature between 45 and 50 °C, then poured into a TSA plate to create a bacterial layer. Ten microliters of each supernatant test sample was spotted on the bacterial layer, and the plates were incubated at 37 °C for 24 h. After incubation, if any clear zones or plaques were observed on the plates, then the plaques were picked using a sterile pipette tip, suspended in 100 μl of Gelatin-SM buffer [5.8 g NaCl, 2.0 g $MgSO_4 \cdot 7H_2O$, 50 mL 1 M Tris-HCl pH 7.4, in 1-liter dH_2O], and stored at 4 °C for 4 h. Subsequently, a tenfold serial dilution of each plaque and spot assay was made on the bacterial host and repeated several times to get a single purified phage. Finally, 10 mL of the bacterial

Rezk *et al. Journal of Genetic Engineering and Biotechnology*   (2022) 20:133

Page 4 of 16

host culture was infected with 100 μl of a single phage to increase the number of Plaque Forming Unit (PFU)/mL, which were measured by spot assay of decimal dilutions.

Phage characterization

Pulsed-field gel electrophoresis (PFGE)

PFGE analysis was used to estimate the genome size of the isolated phage as described by Lingohr et al. [47] with slight modifications. Briefly, 100 μl of phage suspension (10^9 PFU/mL) was mixed with 100 μl of 1.4% of plug agarose. After solidification, the plugs were immersed in lysis buffer (1 mg/mL Proteinase K [ThermoFischer Scientific, USA]); 0.2% w/v SDS [Sigma Aldrich, Gillingham, UK]; and 100 mM EDTA; 1% w/v N-Lauryl sarcosine [Sigma Aldrich, Gillingham, UK] and incubated at 55 °C for 18 h. After incubation, the plugs were washed and added to the PFGE 1.5% agarose gel and Lambda PFG Ladder (Biolabs, UK) was used. The PFGE was run for 18 h at 200 V (6 V/cm) with a 30- to 60-s switch time using a Bio-Rad CHEF DRII system (Biorad, USA). For imaging, 5 μl of ethidium bromide (Carl Roth, Germany) was added to the distilled water, washed, and analyzed under UV light at the Gel Dock imaging system (Biorad, USA).

Host range analysis

The lytic activity of the isolated phage against fifty clinical isolates of *P. aeruginosa* was investigated using the spot assay in triplicate as previously described [46]. The appearance of clear zones (bacterial lysis) confirmed the susceptibility of bacterial strains to the phage in the spotting area.

Phage DNA sequencing

Genomic DNA was extracted from the isolated phage with 10^{10} PFU/mL lysates. According to the manufacturer's instructions, the DNA extraction was performed using proteinase K treatment (100 μg/mL in 10 mM EDTA pH 8), followed by resin purification using the Wizard DNA extraction kit (Promega, UK). The nucleotide sequencing was performed using the Illumina MiSeq platform. Nextera XT DNA Library Preparation Kit was used to prepare the DNA library (Illumina, Cambridge, UK). The paired-end DNA reads were evaluated for accuracy using FASTQC [48]. Moreover, low-quality bases were trimmed using PRINSEQ. Cleaned reads were de novo assembled using SPAdes [49] with multiple K-mers: 21, 33, 55, 77, and 99 . Genome assembly was checked for quality using QUAST [50]. BLASTn against the NCBI Nucleotide database was used to identify closely related phages. Then, the top-matched phages were imported into MEGA-X [51] to draw a phylogenetic tree using CLUSTAL-W aligner [52] and the best Maximum likelihood fit model (GTR: general time

reversible substitution model, G: Gamma distributed among sites). Open-reading frames were predicted using ORF finder. The predicted ORFs were compared against the NCBI non-redundant protein sequences (nr) database using BLASTp to identify putative coding sequences (CDSs). The predicted putative genes were compared to those predicted through PHASTER [53]. The annotated genome of the isolated phage (ZCPA1) has been deposited in the NCBI GenBank under the accession numbers OL597541:OL597590. The genetic map focusing on putative coding genes was generated using SNAPGene (GSL Biotech; available at https://www.snapgene.com/; Access date: 27 July 2021).

Physical stability of phage

The thermal stability of the ZCPA1 with a high titer (10^9 PFU/mL) was performed by incubating tubes containing the phage suspended in SM buffer at 37, 50, 60, 70, and 80 °C for 1 h. After incubation, the phage was enumerated through ten-fold serial dilution and spotted in triplicate by the spot test assay as previously described. Furthermore, the pH stability was investigated using various test tubes containing deionized water with a pH range (2–11) adjusted using HCl and NaOH, and incubated for 1 h [27]. Then, the phage titer was calculated by the spot test assay. In addition, the phage susceptibility against UV inactivation was determined by exposing the phage suspended in SM buffer directly to UV radiation ($\lambda = 253$ nm) for 1 h. A sample was taken for phage enumeration at 10-min intervals using spot test assay in triplicate.

Biofilm clearance assay

The antibiofilm activity of phage was investigated against established (*P.s* 12) biofilm. The methodology was described in previous studies [54, 55]. Briefly, the bacterial culture grown in TSB was supplemented with 0.1% glucose for biofilm enhancement, placed in a 96-well plate as six replicates and left for 48 h to form biofilm at 37 °C. After incubation, phage was added to the formed biofilm with different multiplicity of infections (MOIs): 0, 0.01, 0.1, 1, 10, and 100, and left for another 24 h. Then, the plate was washed to remove any unattached cells. A 1% crystal violet was added to the wells for staining, and 30% glacial acetic acid was used for the quantitative assay using FLUOstar® Omega Microplate Reader at OD_{540} (BMG LABTECH, Germany).

One-step growth curve

As previously described by Taha et al. [56], a one-step growth curve was conducted to determine the different stages of the phage replication cycle. The bacterial culture (*Ps.* 12) was grown in TSB at 10^5 colony forming

unit (CFU/mL), infected by the isolated phage at MOI 1, and incubated at 37 °C for 4 h. During the incubation time, 200-µL aliquots were withdrawn at various time points (0, 10, 20, 30, 45, 60, 90, 120, 180, and 240 min) and divided into two 100-µL samples. A 1% chloroform was added to one of them to determine the eclipse period through releasing the intracellular phages, and another one was left without chloroform. Both samples were ten-fold serially diluted, and the phage titer was enumerated by the spot test assay as previously described.

Time-killing curve
The bacterial reduction was determined using phage ZCPA1 at different MOIs (0.1, 1, 10, 100). One hundred eighty microliters of bacterial culture at 10^6 CFU/mL combined with 20 µL of the phage suspension with different MOIs (0.1, 1, 10, 100). Six replicates were done using 96-well plate. The FLUOstar® Omega plate reader was used for monitoring the OD_{600} changes, and the data were collected at 5 min intervals for 4 h at 37 °C.

Morphological characterization by transmission electron microscopy (TEM)
The phage was imaged using TEM JEOL 1230 in the faculty of science, Alexandria University, Egypt. The phage (10^9 PFU/mL) was prepared in SM buffer and submerged on Formvar carbon-coated copper grids (Pelco International), then stained with 2% phosphor tungstic acid (pH 7.0) and subjected to drying before TEM examination.

Assessment of phage against *P. aeruginosa*-infected wound rat model
Surgical procedures of full-thickness wound model
The solution of phage suspension can be applied locally to the wounded skin area to examine its healing potential on the infected full-thickness excision skin wound in a rat model. The animal experiments were certified by the Animal Care Committee of the Alexandria University (ALEXU-IACUC), with an authorized acceptance for the surgical procedures (AU-IACUC-14/2100601-3-6). This study is reported following ARRIVE guidelines (Animal Research: Reporting of In Vivo Experiments) (https://arriveguidelines.org).

Twenty-five Wistar male rats (8 weeks old), weighing approximately 180–200 g, were selected in the in vivo animal study. The rats were housed individually in a separate stainless-steel cage allowing free access to a standard laboratory diet and mineral water ad libitum. According to formerly published studies, the surgical procedures for the full thickness excision wound were carried out [57–59]. First, the animals were anaesthetized by an intramuscular injection of xylazine (10mg/kg) and ketamine (60 mg/kg). Then, the back hair in the dorsal areas was

removed using an electric shaver. A rounded wound was formed, with a diameter of 15 mm on the dorsal area of the rats using dissecting scissors and sterile forceps. The animals were randomly categorized into five groups with five rats. The first group includes applied sterile gauze (no wound infection) as a positive control. Wound infection was completed by inoculating the wound with *P.s* 12 (1×10^7 CFU/mL) for 2 h before applying the treatment. Both 2nd and 3rd groups were applied sterile gauze as a negative control and gentamicin cream as an antibiotic treatment, respectively. The 4th and 5th groups were applied multi-dose and single-dose phage with 1×10^9 PFU/mL, respectively. A swab for all groups was taken to calculate the bacterial count inhabiting the wound on the 3rd, 7th, 10th, and 14th days post-surgery. The gentamicin and phage (for the multi-dose group) were reapplied each time. Moreover, the wound was rated and photographed via a digital camera. The wound area was estimated using a digital caliper, and the percentage wound closure rate was calculated from the following equation [60, 61]:

$$\text{Wound closure } (\%) = \left[1 - \left(\text{Wound area on given day}/\text{Wound area on day 0}\right)\right] \times 100.$$

Histological examination
On the 17th day, the rats were sacrificed, followed by the removal of the tissue from the wound bed and its surrounding healthy skin to assess the skin wound healing. For histopathological investigations, the tissue was fixed in 10% formaldehyde and embedded in paraffin blocks. The skin sections were stained with hematoxylin and eosin (H&E) and examined under a light microscope (Leica, Germany). A histological examination of the whole wound area was done. The mean value of the percentage of the fibrous tissue, the granulation tissue, and the epidermal thickness was quantified using ImageJ, v1.53 (Maryland, USA). The skin appendages, hair follicles and sebaceous glands, were scored (no skin appendages in wound area= score 1, few <5/wound area = score 2, and ≥5/wound area = score 3). The skin sections were also stained with Masson trichrome staining. Image color deconvolution v1.53 (Maryland, USA) was used to quantify the percentage area of fibrosis in each specimen [62, 63].

Immunohistochemical (IHC) staining and interpretation
IHC of all sections was done using the Avidin-Biotin-Peroxidase method [64]. CD45 (ready to use primary antibody, mouse anti-human, monoclonal antibody, P0042; Leica Biosystems, USA) and α-SMA (ready to use primary antibody, mouse anti-human, monoclonal antibody, P0943; Leica Biosystems, USA) were used to stain the lymphocytes, blood vessels, and myofibroblasts

Rezk *et al. Journal of Genetic Engineering and Biotechnology*   (2022) 20:133

Page 6 of 16

respectively. The antibodies were added to each section using the Bond-Max fully automated immunostainer (Leica Biosystems, USA). Positive control for each primary antibody using tonsil and leiomyoma was added in each run. Negative control omitting the primary antibody was also added in each run. The IHC quantification of CD45 and α-SMA was performed on each slide using the quantitative-image analysis (Leica microsystems, Switzerland).

Statistical analysis

All experiments were conducted in triplicates, and the results were illustrated in the form of mean $\pm$ standard deviation (SD). In this study, GraphPad Prism v5 software was used to generate graphs and perform all statistical analyses. Both Student's *t*-test (two-tailed) and ANOVA tests were used during the work to evaluate the significance $p < 0.05$.

Results

Bacterial characterization

Antibiotic susceptibility is classified into sensitive, intermediate, and resistant (Additional file 1: Table S1). The majority of the bacterial strains showed a high resistance pattern to fluoroquinolones (FQs), with 65 % of levofloxacin resistance and 59 % of ciprofloxacin resistance. These findings indicated that *P. aeruginosa* was more resistant to levofloxacin than ciprofloxacin. Moreover, the *P. aeruginosa* isolates exhibited high resistance to beta-lactams, including 67% resistance to meropenem. Gentamicin demonstrated a high resistance pattern at 63%. Accordingly, 29 of the tested *P. aeruginosa* isolates were MDR bacteria.

Moreover, seven virulence and antibiotic-resistance genes (*Exo A*, *Exo S*, *Phz I and II*, *bla-TEM*, *OprL* and *plcH*) have been identified in the ten resistant *P. aeruginosa* isolates tested using PCR. Furthermore, using BLASTn, the 16S rRNA sequence of *P.s* 12 was found to be 99% identical to *P. aeruginosa* strain B19 16S ribosomal RNA gene, the partial sequence with GenBank Acc. No. MZ425417.1.

Phage characterization
The ZCPA1 phage morphology

According to the morphology of the phage, it belongs to the *Siphoviridae* family. The phage consists of an icosahedral head and a long noncontractile flexible tail. The phage head-to-tail length ratio was similarly typical of the *Siphoviridae* family, with a 66.80-nm width of icosahedral head and 188.54 nm long tail (Fig. 1).
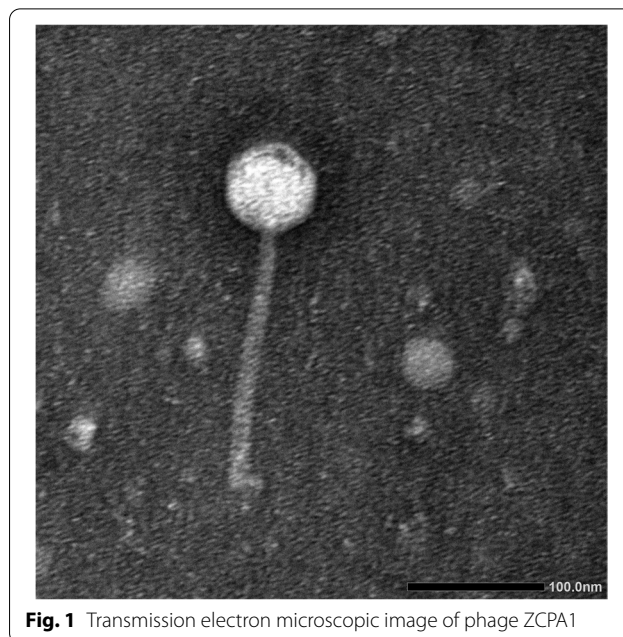
Fig. 1 Transmission electron microscopic image of phage ZCPA1

Host range analysis

The lytic activity of the phage ZCPA1 against different resistant bacterial strains was evaluated. The ZCPA1 exhibited a broad host range with lytic activity against 58% of the tested *P. aeruginosa* clinical isolates (Table 2).

Physical stability of the phage

To use ZCPA1 in therapy, phage stability was examined against various environmental conditions, including heat, pH, and UV. The ZCPA1 exhibited thermal stability at 37 °C with 10^9 PFU/ mL, then decreased gradually to 10^8 PFU/mL at 50 °C and 60 °C. At the same time, it dropped significantly to 10^6 PFU/mL at 70 °C, and the phage was undetectable at 80 °C (Fig. 2A). Moreover, phage ZCPA1 exhibited no significant titer reduction at a wide range of pH values (4–10) with maximum activity at pH 7, and the phage performance was changed after exposure to extreme pH conditions as its infectivity was significantly inactive at pH 2, 3, and 11 (Fig. 2B). In addition, the phage showed resistance to UV inactivation for 45 min under UV light with one log reduction after 1 hour (Fig. 2C).

The phage genome

The genome of phage ZCPA1 has been sequenced and deposited in the GenBank database (GenBank Acc. No. OL597541:OL597590). Phage ZCPA1 contains a double-stranded DNA genome of 46 kbp, which also agreed with the PFGE results. The phage ZCPA1 has an overall G + C content of 64.04%. Moreover, BLASTn analysis

Table 2 The lytic activity of phage ZCPA1 against 50 clinical isolates of *P. aeruginosa* (*P.s* 1 to *P.s* 50)

Bacterial strain	ZCPA1	Bacterial strain	ZCPA1	Bacterial strain	ZCPA1	Bacterial Strain	ZCPA1	Bacterial strain	ZCPA1
P. s 1	+	*P. s* 11	−	*P. s* 21	+	*P. s* 31	+	*P.s* 41	−
P. s 2	−	*P. s* 12	+	*P. s* 22	+	*P. s* 32	+	*P.s* 42	−
P. s 3	+	*P. s* 13	+	*P. s* 23	+	*P. s* 33	+	*P.s* 43	−
P. s 4	−	*P. s* 14	−	*P. s* 24	+	*P. s* 34	+	*P.s* 44	−
P. s 5	−	*P. s* 15	+	*P. s* 25	+	*P. s* 35	−	*P.s* 45	−
P. s 6	−	*P. s* 16	+	*P. s* 26	+	*P. s* 36	+	*P.s* 46	−
P. s 7	−	*P. s* 17	+	*P. s* 27	+	*P. s* 37	+	*P.s* 47	−
P. s 8	−	*P. s* 18	+	*P. s* 28	+	*P. s* 38	+	*P.s* 48	−
P. s 9	−	*P. s* 19	+	*P. s* 29	+	*P.s* 39	+	*P.s* 49	−
P. s 10	−	*P. s* 20	+	*P. s* 30	+	*P.s* 40	−	*P.s* 50	−

+ indicates lysis, and − indicates no lysis

confirmed that ZCPA1 is a member of the *Siphoviridae* family, in the order of *Caudovirales*. Assembly parameters were as follows: contigs# 476, N50 1648, L50 8, N's per 100 kb 0. BLASTn alignment and phylogenetic tree showed that *Pseudomonas* phage vB_PaeS_PcyII-40_PfII40a isolate genome, chromosome (GenBank Acc. No. LT608331.1), was closely related to the genome of ZCPA1 (Fig. 3). The annotated genes were manually curated and listed in Additional file 1: Table S2. The open reading frames (ORFs) prediction applying the standard genetic code identified ninety putative protein-coding genes. The functional genes of phage ZCPA1 are shown in the genetic map (Additional file 1: Figure S1). Among these, forty predicted proteins have assigned functions, involving cell lysis proteins, DNA replication/transcription/repair structural proteins, and DNA packaging proteins. ZCPA1 has fifty ORFs on the leading strand and forty ORFs on the complementary strand.

In vitro characterization of phage ZCPA1
A one-step growth curve determined the replication cycle of the phage ZCPA1 (Fig. 4A). The IC refers to the phage infective centers, indicating the number of free virions released from the bacterial cells without the addition of chloroform, while PFU indicates the number of virions inside and outside the bacterial cell due to chloroform addition. The latent phage period was estimated to be about 90 min, in which the phage virions were naturally released from the bacterial host. The eclipse period of the phage was about 45 min, which indicates the required time for viral particles to be synthesized and assembled since the bacterial lysis was aided by chloroform addition. The burst size was calculated at about 68 virions per single bacterium.

The lytic activity of phage against *P.s* 12 was tested at different MOIs (0.1, 1, 10, 100). During the first 3h, the bacterial turbidities at OD_{600} were 0.295 ±0.02 for bacterial control, 0.264 ±0.03 for MOI 0.1, 0.242 ±0.01 for MOI 1, 0.056 ±0.005 for MOI 10, and around 0 for MOI 100. However, after 4 h-incubation, the media turbidity changed to OD_{600} values of 0.72, 0.70, 0.493, 0.09, and around 0 for the control bacteria (bacteria without phage treatment) and the bacteria treated with phage at various MOIs, in the same order as described above. (Fig. 4B). As a result, the optimum MOI of the phage ZCPA1 is 10.

Biofilm clearance assay
Besides, the phage ZCPA1 exhibited a high level of reduction in the *P.s* 12 biofilm biomass, starting from low MOIs of 0.1 to high MOIs of 100. At OD_{540}, the established biofilm biomass by *P.s* 12 was 1.67, 1.47, 0.23, 0.11, 0.09, and 0.12 for the -ve control and phage with MOI of 0.01, 0.1, 1, 10, and 100, respectively (Fig. 5).
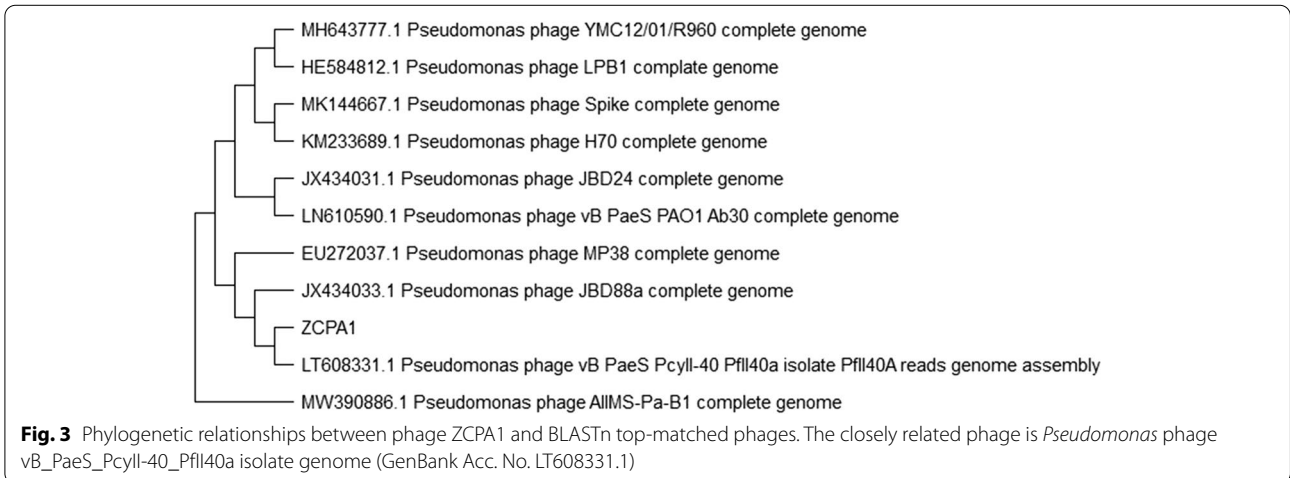
In vivo wound healing
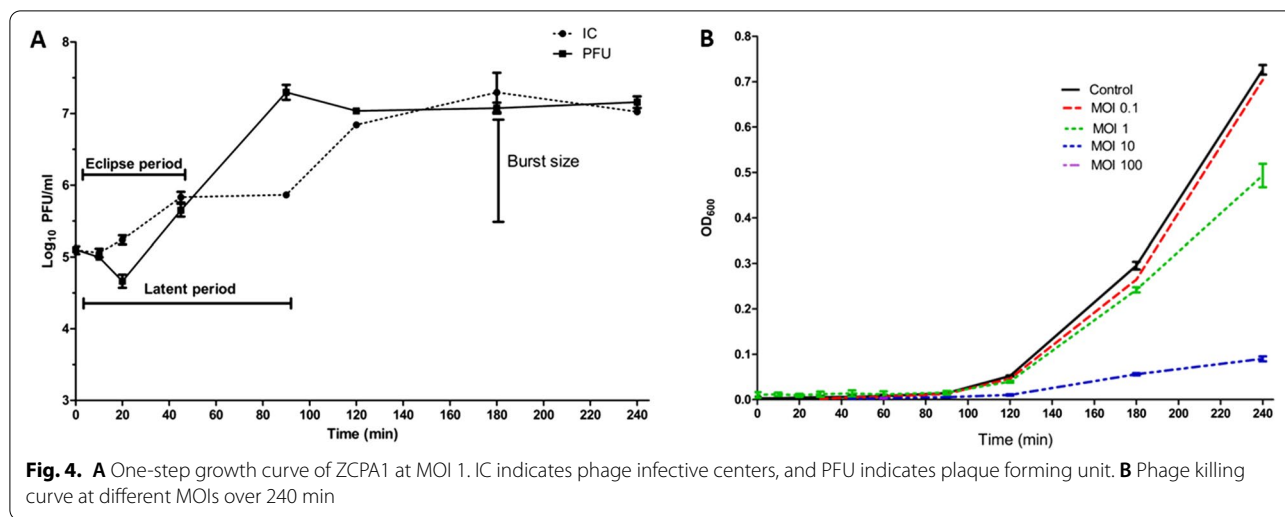#### *Photodocumentary analysis and wound healing percentage*
The wound closure percentage, bacterial count, and histopathological analysis throughout 17 days indicate that the phage ZCPA1 is a promising antibacterial agent against the MDR *P. aeruginosa* with high-quality wound healing in a full-thickness wound infection in a rat model. Figure 6A and B display the percentage of wound closure, which is critical for the successful repair of wound tissues. By day 17, both phage-treated groups showed prompt epithelialization of the wound area, evidenced by a higher percentage of wound closure of 99.84% and 99.93% for the groups in which phage was applied in single and multiple doses, respectively. On the other hand, the negative control group that applied sterile gauze showed a lower percentage of wound closure (69.66%). In addition, the gentamicin-treated group exhibited expansion and enlargement of the wound area, resulting in non-healing wounds with purulence and foul odor. The bacterial count

Rezk *et al. Journal of Genetic Engineering and Biotechnology*   (2022) 20:133

Page 8 of 16
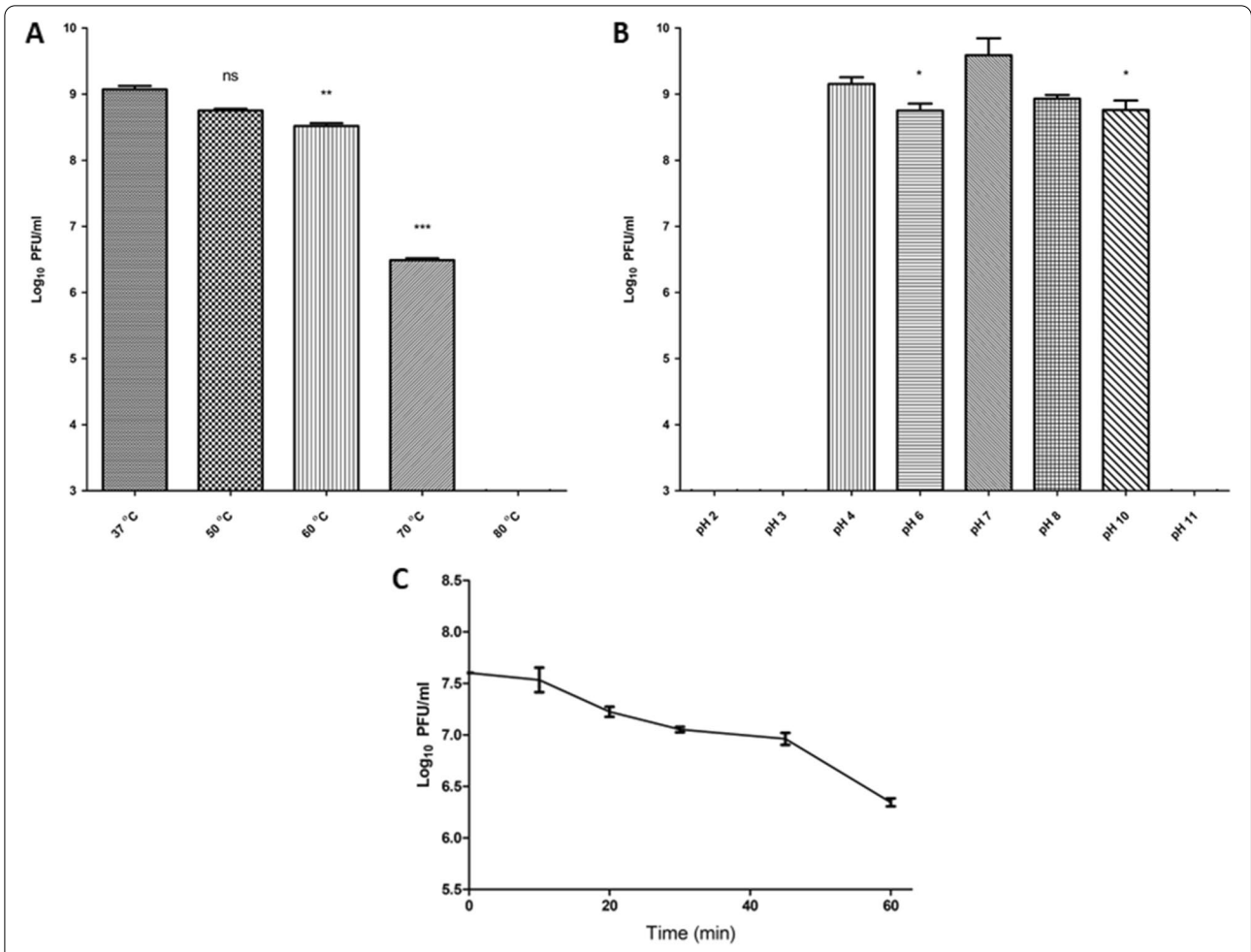
Fig. 2 The physical stability of the phage ZCPA1. **A** Phage viability at different temperatures, **B** phage viability at different pH values, and **C** phage viability under UV light ($\lambda = 253$ nm). ns stands for no significance, $*P < 0.05$, $**P < 0.01$, and $***P < 0.001$
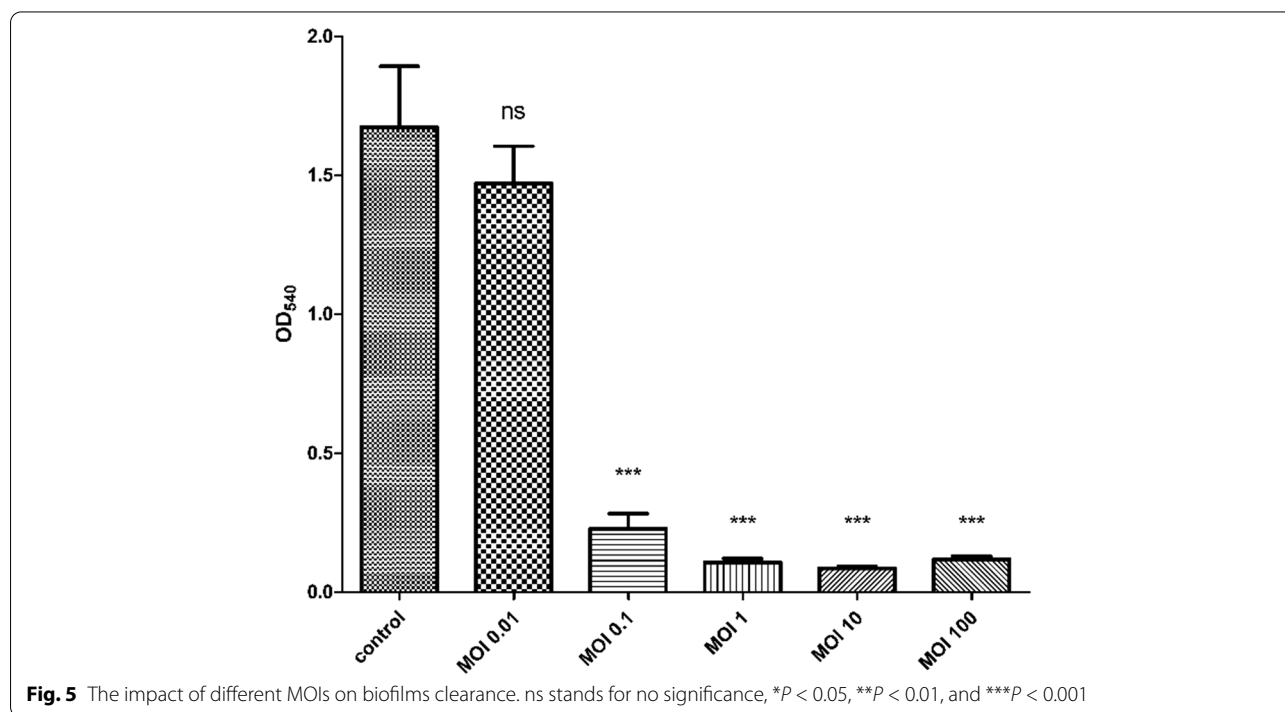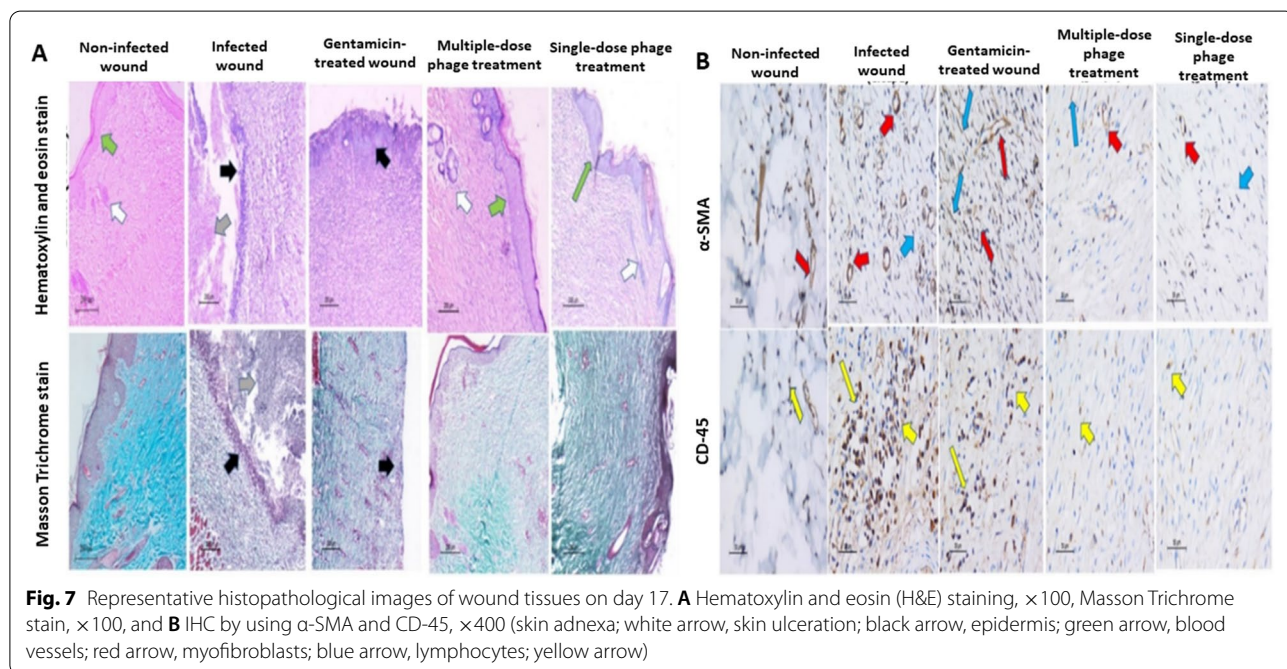

Fig. 3 Phylogenetic relationships between phage ZCPA1 and BLASTn top-matched phages. The closely related phage is *Pseudomonas* phage vB_PaeS_Pcyll-40_Pfll40a isolate genome (GenBank Acc. No. LT608331.1)

Rezk *et al. Journal of Genetic Engineering and Biotechnology*   (2022) 20:133

Page 9 of 16

Fig. 4. **A** One-step growth curve of ZCPA1 at MOI 1. IC indicates phage infective centers, and PFU indicates plaque forming unit. **B** Phage killing curve at different MOIs over 240 min
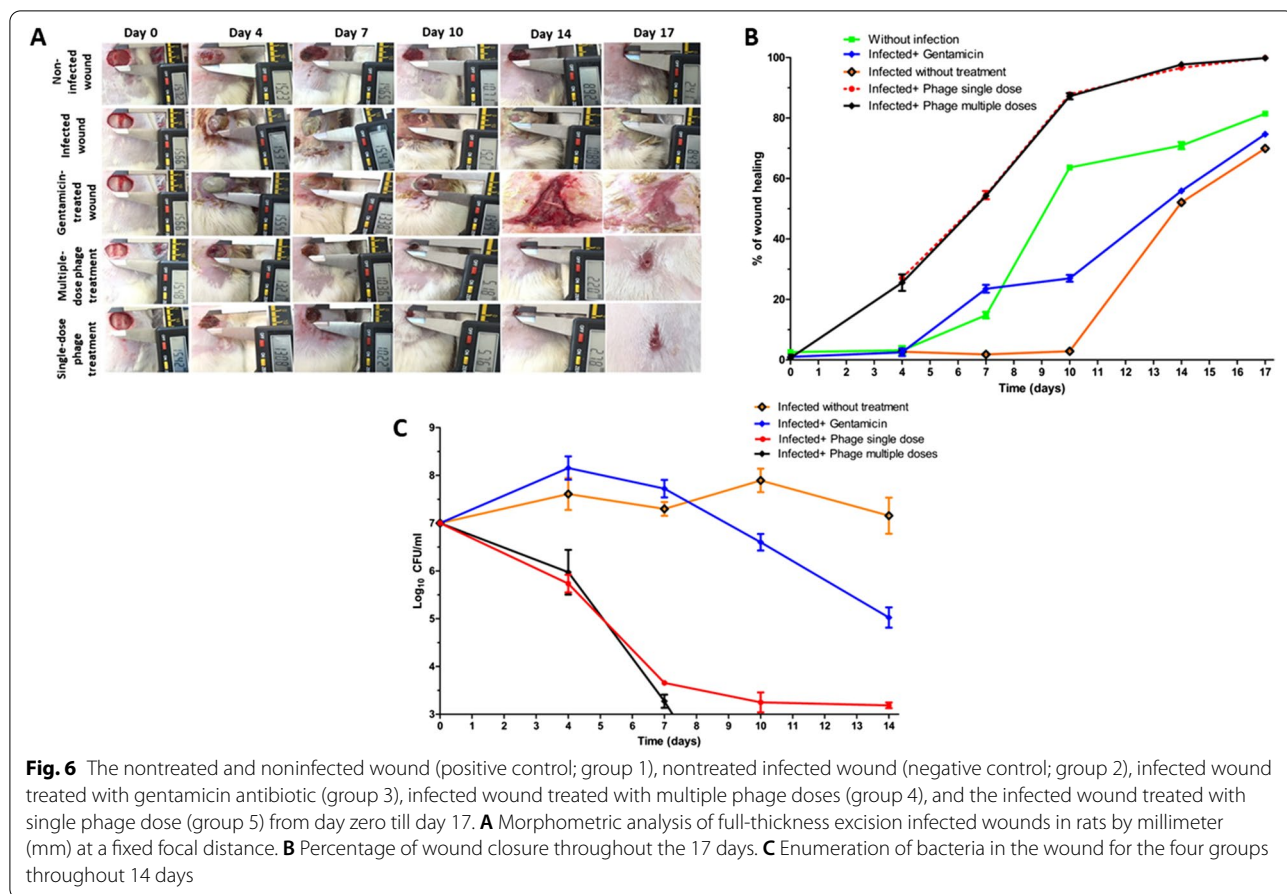
of the wounds for all the groups was investigated throughout the 14 days. According to Fig. 6C, the detection limit was 10^2 CFU/mL. The single phage dose showed a 4 $\log_{10}$ reduction, while multiple phage doses exhibited more than 4 $\log_{10}$ reductions in the total bacterial count. In contrast, the gentamicin-treated wound showed a 2 $\log_{10}$ reduction compared to the positive control.

Histopathological analysis of wound healing

Figure 7 shows skin specimen from the positive control group (group 1) exhibited epidermal re-epithelialization

(green arrow) 52.3±0.4 μm with the regeneration of the appendages ≥5/wound area (score 3) (evidenced by H&E staining ×100). The dermis was formed predominantly of collagen fibers and fibrous tissue 95.3±3.2% (remodeling phase) (highlighted by the Masson's trichrome stain ×100). The granulation tissue was minimal and formed of few newly formed blood vessels 6±2.1/HPF, few myofibroblasts 7±1.2/HPF (highlighted by the immunohistochemistry for α-SMA, ×400), and few lymphocytes 6±2.0/HPF (highlighted by the immunohistochemistry for CD-45, ×400). Skin specimen from the negative

Fig. 5 The impact of different MOIs on biofilms clearance. ns stands for no significance, $*P < 0.05$, $**P < 0.01$, and $***P < 0.001$

Fig. 6 The nontreated and noninfected wound (positive control; group 1), nontreated infected wound (negative control; group 2), infected wound treated with gentamicin antibiotic (group 3), infected wound treated with multiple phage doses (group 4), and the infected wound treated with single phage dose (group 5) from day zero till day 17. **A** Morphometric analysis of full-thickness excision infected wounds in rats by millimeter (mm) at a fixed focal distance. **B** Percentage of wound closure throughout the 17 days. **C** Enumeration of bacteria in the wound for the four groups throughout 14 days

Fig. 7 Representative histopathological images of wound tissues on day 17. **A** Hematoxylin and eosin (H&E) staining, ×100, Masson Trichrome stain, ×100, and **B** IHC by using α-SMA and CD-45, ×400 (skin adnexa; white arrow, skin ulceration; black arrow, epidermis; green arrow, blood vessels; red arrow, myofibroblasts; blue arrow, lymphocytes; yellow arrow)

control group (group 2) showed extensive epidermal ulceration and crust formation 34±3.2, lacking skin appendages (H&E staining ×100). The dermis showed an excessive number of inflammatory cells (inflammatory phase) and a minimal amount of fibrous tissue (highlighted by the Masson's trichrome stain ×100) 2.1±0.3%. The granulation tissue was formed of newly formed blood vessels 25±2/HPF, myofibroblasts 20.4±2.5/HPF (highlighted by the immunohistochemistry for α-SMA, ×400), and an increased number of lymphocytes 78±4.2/HPF (highlighted by the immunohistochemistry for CD-45, ×400). Skin specimen from gentamicin treated group (group 3) showed epidermis ulceration, lacking skin appendages (evidenced by H&E staining ×100). The dermis demonstrated the inflammatory healing phase formed of few amounts of fibrous tissue (highlighted by the Masson's trichrome stain ×100) 7.8±3.5%, an increased amount of granulation tissue formed of newly formed blood vessels 40±1.6/HPF, myofibroblasts 32±6.3/HPF (highlighted by the immunohistochemistry for α-SMA, ×400), and the number of lymphocytes 40±3.7/HPF (highlighted by the immunohistochemistry for CD-45, ×400). Skin specimen from multiple phage doses treatment (group 4) showed epidermal re-epithelialization of thick epidermis 61.2±1.2 μm with the regeneration of the skin appendages ≥5/wound area (score 3), (evidenced by H&E staining ×100). The dermis demonstrated the remodeling phase of wound healing formed mainly of collagen fibers 99±0.6% (highlighted by the Masson's trichrome stain ×100) and a minimal amount of granulation tissue formed of newly formed blood vessels 2±0.4/HPF, myofibroblasts 1.4±0.3/HPF (highlighted by the immunohistochemistry for α-SMA, ×400), and lymphocytes 3±0.3/HPF (highlighted by the immunohistochemistry for CD-45, ×400).

Skin specimen from single phage dose treatment (group 5) displayed the epidermal re-epithelialization of thick epidermis 58±1.8 μm with the regeneration of the skin appendages ≥5/wound area (score 3) (evidenced by H&E staining ×100). The dermis was in the remodeling phase of wound healing, formed mainly of collagen fibers (highlighted by the Masson's trichrome stain ×100) 97.3±2.3%, and a minimal amount of granulation tissue formed of newly formed blood vessels, 4±1/HPF, myofibroblasts 3±1.4/HPF, (highlighted by the immunohistochemistry for α-SMA, ×400), and lymphocytes 5±2.2/HPF (highlighted by the immunohistochemistry for CD-45, ×400).

Discussion

Due to the misuse of antibiotics in clinical therapy, bacteria have evolved resistance against most commercial antibiotics. Many studies have demonstrated that phages are one of the most potent weapons for eradicating *P. aeruginosa* biofilms and planktonic cells due to their natural abundance, specificity, and safety [65].

This study isolated 50 clinical isolates of *P. aeruginosa* from Egyptian hospitalized patients and screened for antibiotic sensitivity. Their antibiotic profile indicated that the isolated *P. aeruginosa* were more resistant to levofloxacin than ciprofloxacin, which agreed with Zhao et al. [66]. FQs are the most commonly used antibiotics against *P. aeruginosa* infections; however, *P. aeruginosa* acquires resistance to the FQs through overexpression of efflux pumps and point mutations in target site genes [67]. Moreover, the tested *P. aeruginosa* isolates exhibited high resistance to β-lactams because of β-lactamase production, especially the AmpC β-lactamase, efflux pump expression, permeability changes, and changes in the target site [5, 68]. Besides, the *P. aeruginosa* isolates revealed high resistance to gentamicin, which agreed with a previous study that showed high aminoglycoside resistance among MDR and extensively drug-resistant (XDR) *P. aeruginosa* clinical isolates in Egypt [69]. Another study showed that the primary mechanism of resistance against aminoglycoside is methyltransferases responsible for changing the drug-binding sites [70]. Accordingly, 29 of the tested *P. aeruginosa* isolates in this study were MDR bacteria [71]. Seven virulence and antibiotic resistance of the tested *P. aeruginosa* isolates were confirmed using PCR, involving *Exo A*, *Exo S*, *Phz I and II*, *bla-TEM*, *OprL*, and *plcH*. Exo A gene is exotoxin A, which is responsible for local tissue damage and invasion of infection [72]. At the same time, the production of *Exo S* was recently linked to chronic infections as it causes cell necrosis, inhibition of DNA synthesis, and endocytosis [73]. In addition, *PhzI* and *PhzII* are required for pyocyanin production, which destroys the host cells and is essential for biofilm formation [74].

Moreover, the *Bla-TEM* gene indicates β-lactam resistance [75]. *OprL* is an essential component of the outer membrane of the bacterial cell, which maintains its integrity and is considered a marker for identifying *P. aeruginosa*-associated infections [76]. In addition, *PlcH* encodes a hemolytic toxin that destroys cell membranes and phospholipids [77]. According to the antibiotic profile and virulence genes, *P.s* 12 was chosen as a multi-drug resistant bacterial host for phage isolation and further studies. The phage ZCPA1 was isolated from raw sewage water sampled from Giza, Egypt, and both morphological analysis by TEM and genome sequencing confirmed that it belongs to the *Siphoviridae* family. The host range, physical stability against harsh environmental conditions, and lytic activity against planktonic and biofilm biomass of potential therapeutic phages are critical for ensuring their efficacy in being a good therapeutic

Rezk *et al. Journal of Genetic Engineering and Biotechnology*   (2022) 20:133

Page 12 of 16

agent. The potential phage for therapy must withstand a wide range of pH and temperature conditions in clinical and environmental applications [78]. The phage ZCPA1 exhibited a broad host range, which could infect 58% of the tested resistant *P. aeruginosa* clinical strains ($n = 50$). In addition, it showed good stability at a wide range of temperatures (37, 50, 60, and 70 °C) and a wide range of pH values (4–10). According to De Plano et al., the capsid structure of phages has been proposed for their resistance to harsh physical and chemical conditions, including pH and heat [79]. Besides, the reduction in phage titer at harsh pH conditions is due to the aggregation of viral particles, as shown by Langlet et al. [80]. Also, the phage ZCPA1 showed stability against UV light, which could be due to its linear double-stranded DNA. The type and organization of the phage genome can significantly affect the resistance of phage to UV inactivation. For example, phages with circular single-stranded DNA are more sensitive than those with linear single-stranded RNA. Those with linear double-stranded DNA exhibited the highest photoreactivation following UV exposure [81, 82].

Regarding the replication dynamics of phage ZCPA1, the one-step curve indicated that the latent period was about 90 min that could be relatively long compared to *Pseudomonas* phage DRL-P1 in a study by Sharma et al. [83]. Therefore, it could be explained that bacterial density is inversely proportional to the latent phage period since the low bacterial concentration led to a long phage latent period [84]. In this study, the ability of the phage to reduce the bacterial growth of *P.s* 12 was tested by a time-killing curve at different MOIs (0.1, 1, 10, 100). Based on the obtained results, the MOI 0.1 exhibited a negligible reduction in bacterial growth ($p > 0.05$), while starting from MOI 1, there was a significant bacterial reduction ($p < 0.01$). The highest level of bacterial reduction was observed at MOIs 10 and 100 ($p < 0.001$).

P. aeruginosa biofilm formation is a critical factor in pathogenicity and antimicrobial resistance [83]. It is also considered critical in delaying wound healing and leading to chronic wound infections [85]. As a result, the lytic activity of the phage ZCPA1 was evaluated against the established biofilm by *P.s* 12. Accordingly, at MOI 0.01, there was an insignificant reduction in the bacterial biofilm biomass ($p > 0.05$). However, at MOIs 0.1, 1, 10, and 100, there was about a 95% reduction in bacterial biofilm biomass ($p < 0.001$). According to these data, the phage ZCPA1 can significantly eradicate *P. aeruginosa* planktonic cells and biofilms. These findings agreed with previous studies [25]. According to Adnan et al., after 6-h treatment with MA-1 phage, it exhibited a significant (99.9%) reduction of 74-h-old biofilms compared to control [86]. In another study, the researchers isolated the AZ1 phage and tested its anti-biofilm activity, and the

results showed about 99.9% reduction of 48-h-old biofilm biomass compared to the control [87]. As a result, the phages could have significant anti-biofilm activity. The ability of the phage to break down the biofilm structure is due to encoding a wide range of enzymes, including depolymerases and lysins. The depolymerases can specifically bind and degrade the exopolysaccharide of the host bacterial cells, disturbing the biofilm to facilitate the phage penetration to the bacterial cells. In addition, lysins are hydrolases encoded in the late stage of the lytic cycle of phage infection. They break down the peptidoglycans in the bacterial cell wall, releasing phage progenies from host cells and causing lysis and death [26].

In this study, the therapeutic efficiency of phage ZCPA1 was assessed on rats to treat full-thickness wounds infected with *P.s* 12. The wound closure percentage, bacterial count, and histopathological analysis throughout 17 days indicate that the phage ZCPA1 could be a promising antibacterial agent against the MDR *P. aeruginosa* with high-quality wound healing in a full-thickness wound infection in a rat model. Multiple research studies conducted in vivo experiments to study phages' therapeutic effect and safety against a wide range of MDR bacteria. They exhibited significant results for killing the bacteria with minimal side effects [88–90]. Moreover, the efficacy of phage therapy against MDR *P. aeruginosa* in animal models was investigated. The researchers showed that phage could lead to a complete reduction of the bacterial count, inhibition of biofilm formation, and improvement of wound healing [25, 28, 34–37, 88, 91, 92].

Consequently, the influence of a topical application of phage ZCPA1, administered as single or multiple doses versus gentamicin antibiotic, was investigated in a rat model with *P. aeruginosa*-infected full-thickness excision wound. Skin regeneration, including restoring tissue integrity and function, is the most challenging aspect of wound treatment, as shown by Tottoli et al. [93]. However, the results in this study were promising as photo documentation and bacterial count demonstrated that the phage administration, either single-dose or multi-dose, resulted in 100% bacterial eradication and wound closure. Furthermore, the equivalent results between single-dose and multi-dose phage treatment underlined its self-replicating nature in the presence of susceptible microorganisms, a highly desired characteristic for any antibacterial drug [94].

Furthermore, re-epithelization is critical to successful wound healing [95]. According to the results of our histopathological analysis, both the single-dose and multiple-dose phage-treated rats showed epidermal re-epithelialization of the thick epidermis with the regeneration of the skin appendage similar to the uninfected-wound rats (positive control). In contrast, the

gentamicin-treated rats showed epidermis ulceration, lacked skin appendages, and the infected rats without treatment (negative control) exhibited extensive epidermal ulceration and crust formation without skin appendages. According to Yousefpour et al., exposure of the *P. aeruginosa* to the sub-MIC dose of gentamicin showed increased bacterial virulence due to the antibiotic stress [96]. As the infected wound showed a healing delay in the infected group without treatment and the gentamicin-treated group, bacterial resistance can develop significant wound delay with serious complications. Moreover, we recommend extending this experiment to evaluate the efficacy of antibiotics to which the bacterial strain is sensitive, for example, imipenem, as the positive control. In addition, we can study the synergetic effect of phage when combined with two types of antibiotics, one to which the bacterial strain is sensitive and another is resistant as recent publications are recommending the combination therapy [97, 98].

The results of this study have shown the potential of phage for controlling full-thickness excision wounds caused by *P. aeruginosa.* It is recommended for further studies to study the antibiofilm ability of the phage against established biofilm by *P. aeruginosa* on the wound-infected rat model.

Conclusions

The emergence of antibiotic resistance has led researchers to look for a safe and effective alternative to antibiotics. Phage therapy has exhibited the potential to control the MDR bacteria, such as *P. aeruginosa*. In this study, a novel phage ZCPA1 was isolated and characterized in vitro against MDR *P. aeruginosa*. ZCPA1 is a member of the *Siphoviridae* family, with a wide host range and high temperature, pH, and UV stability. Moreover, it has high lytic activity against MDR *P. aeruginosa* in planktonic and biofilms. The therapeutic efficacy of ZCPA1 was investigated in a full-thickness wound infected with *P. aeruginosa* in a rat model. *P. aeruginosa* inoculated wounds treated with phage showed 100% wound closure, high-quality regeneration, and complete bacterial infection elimination. Therefore, all these properties make phage ZCPA1 a promising therapeutic agent against *P. aeruginosa* skin wound infections*. However, more research is required on the phage formulations to be used topically on wound infections and tested in clinical trials.

Abbreviations
MDR: Multi-drug resistant; MOI: Multiplicity of infection; CFU/mL: Colony forming unit/mL; PFU/mL: Plaque forming unit/mL; IC: Phage infective center; IHC: Immunohistochemical.

Supplementary Information

Declarations

Ethics approval and consent to participate
All methods were carried out according to relevant guidelines and regulations and approved by the Institutional Review Board of Animal Care Committee of the Alexandria University (ALEXU-IACUC) (AU-IACUC-14/2100601-3-6 and 1 June 2021). Furthermore, this study is reported according to ARRIVE guidelines (https://arriveguidelines.org).

Consent for publication
Not applicable.

Competing interests
The authors declare no competing interests.

Author details
[1]Center for Microbiology and Phage Therapy, Zewail City of Science and Technology, Giza 12578, Egypt. [2]Center for X-ray and Determination of Structure of Matter, Zewail City of Science and Technology, Giza 12578, Egypt. [3]Department of Chemistry of Natural and Microbial Products, National Research Centre, Dokki, Giza 12622, Egypt. [4]Department of Botany, Faculty of Science, Mansoura University, Mansoura 35516, Egypt. [5]Department of Surgical Pathology, Faculty of Medicine, Alexandria University, Alexandria 21131, Egypt. [6]Microbiology and Immunology Department, Faculty of Pharmacy, October University for Modern Sciences and Arts (MSA), Giza 11787, Egypt. [7]Faculty of Environmental Agricultural Sciences, Arish University, Arish 45511, Egypt.

References
1. Shrivastava SR, Shrivastava PS, Ramasamy J (2018) World Health Organization releases global priority list of antibiotic-resistant bacteria to guide

Rezk *et al. Journal of Genetic Engineering and Biotechnology*   (2022) 20:133

Page 14 of 16

research, discovery, and development of new antibiotics. JMS - J Med Soc 32(1):76–77. https://doi.org/10.4103/jms.jms_25_17

2. Reynolds D, Kollef M (2021) The epidemiology and pathogenesis and treatment of Pseudomonas aeruginosa infections: an update. Drugs 81(18):2117–2131. https://doi.org/10.1007/s40265-021-01635-6

3. Murray CJ et al (2022) Global burden of bacterial antimicrobial resistance in 2019: A systematic analysis. Lancet 6736(21). https://doi.org/10.1016/s0140-6736(21)02724-0

4. World Health Organization, New report calls for urgent action to avert antimicrobial resistance crisis, *Joint News Release*, 2019. https://www.who.int/news/item/29-04-2019-new-report-calls-for-urgent-action-to-avert-antimicrobial-resistance-crisis%0A https://www.who.int/news-room/detail/29-04-2019-new-report-calls-for-urgent-action-to-avert-antimicrobial-resistance-crisis (Accessed 27 Dec 2021).

5. Torrens G et al (2019) Regulation of AmpC-driven β-lactam resistance in Pseudomonas aeruginosa: different pathways, different signaling. mSystems 4(6):e00524-19. https://doi.org/10.1128/mSystems.00524-19

6. Langendonk RF, Neill DR, Fothergill JL (2021) The building blocks of antimicrobial resistance in Pseudomonas aeruginosa: implications for current resistance-breaking therapies. Front Cell Infect Microbiol 11:1–22. https://doi.org/10.3389/fcimb.2021.665759

7. Breidenstein EBM, de la Fuente-Núñez C, Hancock REW (2011) Pseudomonas aeruginosa: all roads lead to resistance. Trends Microbiol 19(8):419–426. https://doi.org/10.1016/j.tim.2011.04.005

8. Thi MTT, Wibowo D, Rehm BHA (2020) Pseudomonas aeruginosa biofilms. Int J Mol Sci 21(22):1–25. https://doi.org/10.3390/ijms21228671

9. Hsueh PR, Teng LJ, Yang PC, Chen YC, Ho SW, Luh KT (1998) Persistence of a multidrug-resistant Pseudomonas aeruginosa clone in an intensive care burn unit. J Clin Microbiol 36(5):1347–1351. https://doi.org/10.1128/JCM.36.5.1347-1351.1998

10. Panghal M, Singh K, Kadyan S, Chaudary U, Yadav JP (2015) The analysis of distribution of multidrug resistant pseudomonas and bacillus species from burn patients and burn ward environment. Burns 41(4):812–819. https://doi.org/10.1016/j.burns.2014.10.014

11. Willmann M et al (2014) Analysis of a long-term outbreak of XDR Pseudomonas aeruginosa: a molecular epidemiological study. J Antimicrob Chemother 70(5):1322–1330. https://doi.org/10.1093/jac/dku546

12. del Barrio-Tofiño E, López-Causapé C, Oliver A (2020) Pseudomonas aeruginosa epidemic high-risk clones and their association with horizontally-acquired β-lactamases: 2020 update. Int J Antimicrob Agents 56(6):106196. https://doi.org/10.1016/j.ijantimicag.2020.106196

13. US Department of Health and Human Services and CDC. Antibiotic resistance threats in the United States, *Centers for Disease Control and Prevention*, pp. 1–113, 2019, [Online]. Available: https://www.cdc.gov/drugresistance/biggest_threats.html.

14. Al-Orphaly M et al (2021) Epidemiology of multidrug-resistant Pseudomonas aeruginosa in the Middle East and North Africa, Region. Msphere 6(3). https://doi.org/10.1128/mSphere.00202-21

15. Agwa MM, Sabra S, Atwa NA, Dahdooh HA, Lithy RM, Elmotasem H (2022) Potential of frankincense essential oil-loaded whey protein nanoparticles embedded in frankincense resin as a wound healing film based on green technology. J Drug Delivery Sci Technol:103291. https://doi.org/10.1016/j.jddst.2022.103291

16. Moghadam MT, Khoshbayan A, Chegini Z, Farahani I, Shariati A (2020) Bacteriophages, a new therapeutic solution for inhibiting multidrug-resistant bacteria causing wound infection: lesson from animal models and clinical trials. Drug Des Dev Ther 14:1867–1883. https://doi.org/10.2147/DDDT.S251171

17. Shariati A, Moradabadi A, Azimi T, Ghaznavi-Rad E (2020) Wound healing properties and antimicrobial activity of platelet-derived biomaterials. Sci Rep 10(1):1–9. https://doi.org/10.1038/s41598-020-57559-w

18. Pang Z, Raudonis R, Glick BR, Lin TJ, Cheng Z (2019) Antibiotic resistance in Pseudomonas aeruginosa: mechanisms and alternative therapeutic strategies. Biotechnol Adv 37(1):177–192. https://doi.org/10.1016/j.biotechadv.2018.11.013

19. Al-Wrafy F, Brzozowska E, Górska S, Gamian A (2017) Pathogenic factors of Pseudomonas aeruginosa – the role of biofilm in pathogenicity and as a target for phage therapy. Postępy Higieny i Medycyny Doświadczalnej 71(1):78–91. https://doi.org/10.5604/01.3001.0010.3792

20. Malone M et al (2017) The prevalence of biofilms in chronic wounds: a systematic review and meta-analysis of published data. J Wound Care 26(1):20–25. https://doi.org/10.12968/jowc.2017.26.1.20

21. Gajula B, Munnamgi S, Basu S (2020) How bacterial biofilms affect chronic wound healing: a narrative review. Int J Surg: Glob Health 3(2):e16–e16. https://doi.org/10.1097/GH9.0000000000000016

22. Ijaz M, Siddique AB, Rasool MH, Shafique M (2019) Frequency of multi drug resistant Pseudomonas aeruginosa in different wound types of hospitalized patients. Pak J Pharm Sci 32(2):865–870 [Online]. Available: http://www.ncbi.nlm.nih.gov/pubmed/31103984

23. Navarro F, Muniesa M (2017) Phages in the human body. Front Microbiol 8:566. https://doi.org/10.3389/fmicb.2017.00566

24. El-Shibiny A, Dawoud A (2020) Bacteriophage applications for food safety. In: Witzany G (ed) Biocommunication of phages. Springer International Publishing, Cham, pp 463–484

25. Chegini Z, Khoshbayan A, Taati Moghadam M, Farahani I, Jazireian P, Shariati A (2020) Bacteriophage therapy against Pseudomonas aeruginosa biofilms: a review. Ann Clin Microbiol Antimicrob 19(1):1–17. https://doi.org/10.1186/s12941-020-00389-5

26. Ferriol-González C, Domingo-Calap P (2020) Phages for biofilm removal. Antibiotics 9(5):268. https://doi.org/10.3390/antibiotics9050268

27. Abdelrahman F et al (2022) Isolation, characterization, and genomic analysis of three novel E. coli bacteriophages that effectively infect E. coli O18. Microorganisms 10(3):589. https://doi.org/10.3390/microorganisms10030589

28. Heo YJ, Lee YR, Jung HH, Lee J, Ko GP, Cho YH (2009) Antibacterial efficacy of phages against Pseudomonas aeruginosa infections in mice and Drosophila melanogaster. Antimicrob Agents Chemother 53(6):2469–2474. https://doi.org/10.1128/AAC.01646-08

29. Silva C et al (2021) The history and applications of phage therapy in Pseudomonas aeruginosa. Microbiol Res 13(1):14–37. https://doi.org/10.3390/microbiolres13010002

30. Gutiérrez D, Vandenheuvel D, Martínez B, Rodríguez A, Lavigne R, García P (2015) Two phages, phiIPLA-RODI and phiIPLA-C1C, lyse mono-and dual-species staphylococcal biofilms. Appl Environ Microbiol 81(10):3336–3348. https://doi.org/10.1128/AEM.03560-14

31. Chan B, Abedon S (2014) Bacteriophages and their enzymes in biofilm control. Curr Pharm Des 21(1):85–99. https://doi.org/10.2174/1381612820666140905112311

32. Oliveira VC et al (2020) Identification and characterization of new bacteriophages to control multidrug-resistant Pseudomonas aeruginosa biofilm on endotracheal tubes. Front Microbiol 11:2401. https://doi.org/10.3389/fmicb.2020.580779

33. Sharma S et al (2021) Isolation and characterization of a lytic bacteriophage against Pseudomonas aeruginosa. Sci Rep 11(1):19393. https://doi.org/10.1038/s41598-021-98457-z

34. Forti F et al (2018) Design of a broad-range bacteriophage cocktail that reduces pseudomonas aeruginosa biofilms and treats acute infections in two animal models. Antimicrob Agents Chemother 62(6). https://doi.org/10.1128/AAC.02573-17

35. Waters EM et al (2017) Phage therapy is highly effective against chronic lung infections with Pseudomonas aeruginosa. Thorax 72(7):666–667. https://doi.org/10.1136/thoraxjnl-2016-209265

36. Yang X, Haque A, Matsuzaki S, Matsumoto T, Nakamura S (2021) The efficacy of phage therapy in a murine model of Pseudomonas aeruginosa pneumonia and sepsis. Front Microbiol 12(July):1–9. https://doi.org/10.3389/fmicb.2021.682255

37. Holguín AV et al (2015) Phage ΦPan70, a putative temperate phage, controls pseudomonas aeruginosa in planktonic, biofilm and burn mouse model assays. Viruses 7(8):4602–4623. https://doi.org/10.3390/v7082835

38. McVay CS, Velásquez M, Fralick JA (2007) Phage therapy of Pseudomonas aeruginosa infection in a mouse burn wound model. Antimicrob Agents Chemother 51(6):1934–1938. https://doi.org/10.1128/AAC.01028-06

39. Golkar Z (2013) Experimental phage therapy on multiple drug resistant Pseudomonas aeruginosa infection in mice. J Antivirals Antiretrovirals 05(06). https://doi.org/10.4172/jaa.s10-005

40. Nitz F et al (2021) Molecular detection of drug-resistance genes of blaoxa-23-blaoxa-51 and mcr-1 in clinical isolates of pseudomonas aeruginosa. Microorganisms 9(4):1–17. https://doi.org/10.3390/microorganisms9040786

Rezk *et al. Journal of Genetic Engineering and Biotechnology*   (2022) 20:133

Page 15 of 16

41. Haghi F, Zeighami H, Monazami A, Toutouchi F, Nazaralian S, Naderi G (2018) Diversity of virulence genes in multidrug resistant Pseudomonas aeruginosa isolated from burn wound infections. Microb Pathog 115:251–256. https://doi.org/10.1016/j.micpath.2017.12.052

42. Fazeli N, Momtaz H (2014) Virulence gene profiles of multidrug-resistant pseudomonas aeruginosa isolated from Iranian hospital infections. Iran Red Crescent Med J 16(10):15722. https://doi.org/10.5812/ircmj.15722

43. CLSI (2019) CLSI M100-ED29: 2019 performance standards for antimicrobial susceptibility testing, 29th edition

44. Treves DS (2010) Review of three DNA analysis applications for use in the microbiology or genetics classroom. J Microbiol Biol Educ 11(2):186–187. https://doi.org/10.1128/jmbe.v11i2.205

45. Abdelsattar AS, Dawoud A, Makky S, Nofal R, Aziz RK, El-Shibiny A (2021) Bacteriophages: from isolation to application. Curr Pharm Biotechnol 23(3):337-360. https://doi.org/10.2174/138920102266621042609 2002.

46. Mazzocco A, Waddell TE, Lingohr E, Johnson RP (2009) Enumeration of bacteriophages by the direct plating plaque assay. In: Clokie MRJ, Kropinski AM (eds) Methods in molecular biology (Clifton, N.J.), vol. 501. Humana Press, Totowa, pp 77–80

47. Lingohr E, Frost S, Johnson RP (2009) Determination of bacteriophage genome size by pulsed-field gel electrophoresis. In: Clokie MRJ, Kropinski AM (eds) *Methods in molecular biology (Clifton, N.J.)*, vol. 502. Humana Press, Totowa, pp 19–25

48. Brown J, Pirrung M, Mccue LA (2017) FQC dashboard: integrates FastQC results into a web-based, interactive, and extensible FASTQ quality control tool. Bioinformatics 33(19):3137–3139. https://doi.org/10.1093/bioin formatics/btx373

49. Bankevich A et al (2012) SPAdes: a new genome assembly algorithm and its applications to single-cell sequencing. J Comput Biol 19(5):455–477. https://doi.org/10.1089/cmb.2012.0021

50. Gurevich A, Saveliev V, Vyahhi N, Tesler G (2013) QUAST: quality assessment tool for genome assemblies. Bioinformatics 29(8):1072–1075. https://doi.org/10.1093/bioinformatics/btt086

51. Kumar S, Stecher G, Li M, Knyaz C, Tamura K (2018) MEGA X: molecular evolutionary genetics analysis across computing platforms. Mol Biol Evol 35(6):1547–1549. https://doi.org/10.1093/molbev/msy096

52. Thompson JD, Higgins DG, Gibson TJ (1994) CLUSTAL W: improving the sensitivity of progressive multiple sequence alignment through sequence weighting, position-specific gap penalties and weight matrix choice. Nucleic Acids Res 22(22):4673–4680. https://doi.org/10.1093/nar/22.22.4673

53. Furuno M et al (2003) CDS annotation in full-length cDNA sequence. Genome Res 13(6 B):1478–1487. https://doi.org/10.1101/gr.1060303

54. O'Toole GA (2010) Microtiter dish biofilm formation assay. J Vis Exp (47). https://doi.org/10.3791/2437

55. Fong SA et al (2017) Activity of bacteriophages in removing biofilms of pseudomonas aeruginosa isolates from chronic rhinosinusitis patients. Front Cell Infect Microbiol 7:1–11. https://doi.org/10.3389/fcimb.2017.00418

56. Taha OA, Connerton PL, Connerton IF, El-Shibiny A (2018) Bacteriophage ZCKP1: a potential treatment for Klebsiella pneumoniae isolated from diabetic foot patients. Front Microbiol 9. https://doi.org/10.3389/fmicb.2018.02127

57. El-Aassar MR, Ibrahim OM, Fouda MMG, El-Beheri NG, Agwa MM (2020) Wound healing of nanofiber comprising Polygalacturonic/hyaluronic acid embedded silver nanoparticles: in-vitro and in-vivo studies. Carbohydr Polym 238:116175. https://doi.org/10.1016/j.carbpol.2020.116175

58. El-Aassar MR et al (2021) Antibiotic-free combinational hyaluronic acid blend nanofibers for wound healing enhancement. Int J Biol Macromol 167:1552–1563. https://doi.org/10.1016/j.ijbiomac.2020.11.109

59. Shalaby M, Agwa M, Saeed H, Khedr SM, Morsy O, El-Demellawy MA (2020) Fish scale collagen preparation, characterization and its application in wound healing. J Polym Environ 28(1):166–178. https://doi.org/10.1007/s10924-019-01594-w

60. Hasanin M, Swielam EM, Atwa NA, Agwa MM (2022) Novel design of bandages using cotton pads, doped with chitosan, glycogen and ZnO nanoparticles, having enhanced antimicrobial and wounds healing effects. Int J Biol Macromol 197:121–130. https://doi.org/10.1016/j.ijbiomac.2021.12.106

61. El-Shanshory AA, Agwa MM, Abd-Elhamid AI, Soliman HMA, Mo X, Kenawy E-R (2022) Metronidazole topically immobilized electrospun nanofibrous scaffold: novel secondary intention wound healing accelerator. Polymers 14(3):454. https://doi.org/10.3390/polym14030454

62. Abramov Y et al (2007) Histologic characterization of vaginal vs. abdominal surgical wound healing in a rabbit model. Wound Repair Regen 15(1):80–86. https://doi.org/10.1111/j.1524-475X.2006.00188.x

63. Park I-S, Chung P-S, Ahn JC (2015) Enhancement of ischemic wound healing by spheroid grafting of human adipose-derived stem cells treated with low-level light irradiation. PLoS One 10(6):1–16. https://doi.org/10.1371/journal.pone.0122776

64. Hsu SM, Raine L, Fanger H (1981) Use of avidin-biotin-peroxidase complex (ABC) in immunoperoxidase techniques: a comparison between ABC and unlabeled antibody (PAP) procedures. J Histochem Cytochem 29(4):577–580. https://doi.org/10.1177/29.4.6166661

65. Pires DP, Vilas Boas D, Sillankorva S, Azeredo J (2015) Phage therapy: a step forward in the treatment of Pseudomonas aeruginosa infections. J Virol 89(15):7449–7456. https://doi.org/10.1128/jvi.00385-15

66. Zhao L, Wang S, Li X, He X, Jian L (2020) Development of in vitro resistance to fluoroquinolones in Pseudomonas aeruginosa. Antimicrob Resist Infect Control 9(1):124. https://doi.org/10.1186/s13756-020-00793-8

67. Agnello M, Finkel SE, Wong-Beringer A (2016) Fitness cost of fluoroquinolone resistance in clinical isolates of pseudomonas aeruginosa differs by type III secretion genotype. Front Microbiol 7:1591. https://doi.org/10.3389/fmicb.2016.01591

68. Ahmed MAS et al (2020) β-Lactamase-mediated resistance in MDR-Pseudomonas aeruginosa from Qatar. Antimicrob Resist Infect Control 9(1):170. https://doi.org/10.1186/s13756-020-00838-y

69. El-Far A et al (2021) High rates of aminoglycoside methyltransferases associated with metallo-beta-lactamases in multidrug-resistant and extensively drug-resistant pseudomonas aeruginosa clinical isolates from a tertiary care hospital in Egypt. Infect Drug Resist 14(26):4849–4858. https://doi.org/10.2147/IDR.S335582

70. Valderrama-Carmona P, Cuartas JH, Carolina Castaño D, Corredor M (2019) The role of Pseudomonas aeruginosa RNA methyltransferases in antibiotic resistance. Pseudomonas Aeruginosa - Armory Within. https://doi.org/10.5772/intechopen.85185

71. Magiorakos AP et al (2012) Multidrug-resistant, extensively drug-resistant and pandrug-resistant bacteria: an international expert proposal for interim standard definitions for acquired resistance. Clin Microbiol Infect 18(3):268–281. https://doi.org/10.1111/j.1469-0691.2011.03570.x

72. Pollack M (1983) The role of exotoxin a in pseudomonas disease and immunity. Rev Infect Dis 5(Suppl 5):S979–S984. https://doi.org/10.1093/clinids/5.supplement_5.s979

73. Jurado-Martín I, Sainz-Mejías M, McClean S (2021) Pseudomonas aeruginosa: an audacious pathogen with an adaptable arsenal of virulence factors. Int J Mol Sci 22(6):1–37. https://doi.org/10.3390/ijms22063128

74. Moradali MF, Ghods S, Rehm BHA (2017) Pseudomonas aeruginosa lifestyle: a paradigm for adaptation, survival, and persistence. Front Cell Infect Microbiol 7:39. https://doi.org/10.3389/fcimb.2017.00039

75. Hosu MC, Vasaikar SD, Okuthe GE, Apalata T (2021) Detection of extended spectrum beta-lactamase genes in Pseudomonas aeruginosa isolated from patients in rural eastern Cape Province, South Africa. Sci Rep 11(1):1–8. https://doi.org/10.1038/s41598-021-86570-y

76. Chand Y et al (2021) Clinical specimens are the pool of multidrug-resistant Pseudomonas aeruginosa harbouring oprL and toxA virulence genes: findings from a tertiary hospital of Nepal. Emerg Med Int 2021:1–8. https://doi.org/10.1155/2021/4120697

77. Bogiel T, Prażyńska M, Kwiecińska-Piróg J, Gospodarek-Komkowska E, Mikucka A (2021) Carbapenem-resistant pseudomonas aeruginosa strains-distribution of the essential enzymatic virulence factors genes. Antibiotics 10(1):1–10. https://doi.org/10.3390/antibiotics10010008

78. Fernández L, Gutiérrez D, García P, Rodríguez A (2019) The perfect bacteriophage for therapeutic applications—a quick guide. Antibiotics 8(3). https://doi.org/10.3390/antibiotics8030126

79. De Plano LM et al (2021) Role of phage capsid in the resistance to UV-C radiations. Int J Mol Sci 22(7):1–12. https://doi.org/10.3390/ijms22073408

80. Langlet J, Gaboriaud F, Gantzer C (2007) Effects of pH on plaque forming unit counts and aggregation of MS2 bacteriophage. J Appl Microbiol 103(5):1632–1638. https://doi.org/10.1111/j.1365-2672.2007.03396.x

Rezk *et al. Journal of Genetic Engineering and Biotechnology*   (2022) 20:133

Page 16 of 16

81. Rodriguez RA, Bounty S, Beck S, Chan C, McGuire C, Linden KG (2014) Photoreactivation of bacteriophages after UV disinfection: role of genome structure and impacts of UV source. Water Res 55:143–149. https://doi.org/10.1016/j.watres.2014.01.065

82. Bae KS, Shin G-A (2016) Inactivation of various bacteriophages by different ultraviolet technologies: development of a reliable virus indicator system for water reuse. Environ Eng Res 21(4):350–354. https://doi.org/10.4491/eer.2016.032

83. Kamali E, Jamali A, Ardebili A, Ezadi F, Mohebbi A (2020) Evaluation of antimicrobial resistance, biofilm forming potential, and the presence of biofilm-related genes among clinical isolates of Pseudomonas aeruginosa. BMC Res Notes 13(1):27. https://doi.org/10.1186/s13104-020-4890-z

84. Abedon ST, Herschler TD, Stopar D (2001) Bacteriophage latent-period evolution as a response to resource availability. Appl Environ Microbiol 67(9):4233–4241. https://doi.org/10.1128/AEM.67.9.4233-4241.2001

85. Percival SL, McCarty SM, Lipsky B (2015) Biofilms and wounds: an overview of the evidence. Adv Wound Care 4(7):373–381. https://doi.org/10.1089/wound.2014.0557

86. Adnan M et al (2020) Isolation and characterization of bacteriophage to control multidrug-resistant Pseudomonas aeruginosa planktonic cells and biofilm. Biologicals 63:89–96. https://doi.org/10.1016/j.biologicals.2019.10.003

87. Jamal M et al (2017) Isolation and characterization of a bacteriophage and its utilization against multi-drug resistant Pseudomonas aeruginosa-2995. Life Sci 190:21–28. https://doi.org/10.1016/j.lfs.2017.09.034

88. Chadha P, Katare OP, Chhibber S (2016) In vivo efficacy of single phage versus phage cocktail in resolving burn wound infection in BALB/c mice. Microb Pathog 99:68–77. https://doi.org/10.1016/j.micpath.2016.08.001

89. Penziner S, Schooley RT, Pride DT (2021) Animal models of phage therapy. Front Microbiol 12:87. https://doi.org/10.3389/fmicb.2021.631794

90. Ngassam-Tchamba C et al (2020) In vitro and in vivo assessment of phage therapy against Staphylococcus aureus causing bovine mastitis. J Glob Antimicrob Resist 22:762–770. https://doi.org/10.1016/j.jgar.2020.06.020

91. Basu S, Agarwal M, Kumar Bhartiya S, Nath G, Kumar Shukla V (2015) An in vivo wound model utilizing bacteriophage therapy of Pseudomonas aeruginosa biofilms. Ostomy Wound Manage 61(8):16–23 [Online]. Available: http://europepmc.org/abstract/MED/26291897

92. Mendes JJ et al (2013) Wound healing potential of topical bacteriophage therapy on diabetic cutaneous wounds. Wound Repair Regen 21(4):595–603. https://doi.org/10.1111/wrr.12056

93. Tottoli EM, Dorati R, Genta I, Chiesa E, Pisani S, Conti B (2020) Skin wound healing process and new emerging technologies for skin wound care and regeneration. Pharmaceutics 12(8). https://doi.org/10.3390/pharmaceutics12080735

94. Kutter E, Kuhl S, Alavidze Z, Blasdel B (2012) Phage therapy: bacteriophages as natural, self-limiting antibiotics, pp 945–956

95. Safferling K et al (2013) Wound healing revised: a novel reepithelialization mechanism revealed by in vitro and in silico models. J Cell Biol 203(4):691–709. https://doi.org/10.1083/jcb.201212020

96. Yousefpour Z, Davarzani F, Owlia P (2021) Evaluating of the effects of sub-MIC concentrations of gentamicin on biofilm formation in clinical isolates of Pseudomonas aeruginosa. Iran J Pathol 16(4):403–410. https://doi.org/10.30699/IJP.20201.524220.2584

97. Segall AM, Roach DR, Strathdee SA (2019) Stronger together? Perspectives on phage-antibiotic synergy in clinical applications of phage therapy. Curr Opin Microbiol 51:46–50. https://doi.org/10.1016/j.mib.2019.03.005

98. Lin Y, Chang RYK, Britton WJ, Morales S, Kutter E, Chan H-K (2018) Synergy of nebulized phage PEV20 and ciprofloxacin combination against Pseudomonas aeruginosa. Int J Pharm 551(1–2):158–165. https://doi.org/10.1016/j.ijpharm.2018.09.024

Publisher's Note

Springer Nature remains neutral with regard to jurisdictional claims in published maps and institutional affiliations.